Use of Artificial Neural Networks to Retrieve TOA SW Radiative Fluxes for the EarthCARE Mission

Carlos Domenech and Tobias Wehr

***Abstract*—The Earth Clouds, Aerosols, and Radiation Explorer (EarthCARE) mission responds to the need to improve the understanding of the interactions between cloud, aerosol, and radiation processes. The fundamental mission objective is to constrain retrievals of cloud and aerosol properties such that their impact on top-of-atmosphere (TOA) radiative fluxes can be determined with an accuracy of 10 $\mathbf{W \cdot m^{-2}}$. However, TOA fluxes cannot be measured instantaneously from a satellite. For the EarthCARE mission, fluxes will be estimated from the observed solar and thermal radiances measured by the Broadband Radiometer (BBR). This paper describes an approach to obtain shortwave (SW) fluxes from BBR radiance measurements. The retrieval algorithms are developed relying on the angular distribution models (ADMs) employed by Clouds and the Earth's Radiant Energy System (CERES) instrument. The solar radiance-to-flux conversion for the BBR is performed by simulating the Terra CERES ADMs using a backpropagation artificial neural network (ANN) technique. The ANN performance is optimized by testing different architectures, namely, feedforward, cascade forward, and a customized-forward network. A large data set of CERES measurements used to resemble the forthcoming BBR acquisitions has been collected. The CERES BBR-like database is sorted by their surface type, sky conditions, and scene type and then stratified by four input variables (solar zenith angle and BBR SW radiances) to construct three different training data sets. Then, the neural networks are analyzed, and the adequate ADM classification scheme is selected. The results of the BBR ANN-based ADMs show SW flux retrievals compliant with the CERES flux estimates.**

***Index Terms*—Angular distribution models (ADMs), anisotropic correction, artificial neural network (ANN), Earth Clouds, Aerosols, and Radiation Explorer (EarthCARE), remote sensing, solar radiative flux.**

I. Introduction

THE Earth Clouds, Aerosols, and Radiation Explore (EarthCARE) is a forthcoming space mission planned by the European and Japanese space agencies which addresses the need to improve the understanding of the interactions between cloud, aerosol, and radiation processes. These elements play a critical role in the Earth's radiative balance. According to the scientific goals established for EarthCARE in the User Consultation Meeting at the ESA-European Space Research Institute (ESRIN), in April 2004, the overarching mission requirement is to constrain retrievals of cloud and aerosol parameters such that their impact on top-of-atmosphere (TOA) broadband (BB) radiative fluxes is accurate to within 10 $\mathrm{W \cdot m^{-2}}$ for a footprint of 100 $\mathrm{km^2}$ [1]. The required accuracy refers to the total radiative flux error, including instrument and unfiltering errors.

TOA fluxes cannot be measured instantaneously and directly from a satellite; instead, they have to be estimated from radiance measurements acquired by the BB Radiometer (BBR) onboard the EarthCARE spacecraft. The BBR provides quasi-instantaneous measurements of BB reflected solar and emitted thermal TOA radiances of the same target at three fixed viewing angles: nadir, fore, and aft views (along track (AT) at $\pm 50^{\circ}$). This additional angular information on the radiation field can be exploited to construct radiance-to-flux inversion schemes more accurate than those using a single radiance. This paper describes a promising approach to obtain instantaneous radiative shortwave (SW) fluxes from BBR radiance measurements.

II. BBR Flux-Retrieval Algorithm Development

A robust and reliable TOA radiance-to-flux conversion methodology has to be developed for the BBR prior to mission launch so that the retrieval algorithm would be available from day one of the EarthCARE mission in orbit. Thus, the method has to be based on well-proven methods, such as making use of the so-called angular distribution models (ADMs) [2], [3]. These models cannot achieve the required EarthCARE radiative accuracy for all-sky conditions. However, they are consistent with the instantaneous TOA flux accuracy of current Earth-radiation budget missions. ADMs describe the angular dependence of the TOA Earth's radiation field, however, involve errors related to the departures of the instantaneous local anisotropy from the mean anisotropy represented by the ADM. Empirical and theoretical angular models can be used to define the BBR flux-conversion procedure. The former consists in using accumulated satellite data and existing conversion procedures, and the latter is based on radiative-transfer (RT) simulations to relate modeled radiances to corresponding fluxes.

Domenech *et al.* [4], [5] developed theoretical angular models for the BBR, where anisotropic coefficients are retrieved from RT Monte Carlo simulations to construct a synthetic ADM specifically defined for the multipointing capability of the BBR. The comparison between flux estimates obtained with the BBR theoretical models and the empirical methods were not totally satisfactory, and the conclusions stated that

Manuscript received May 19, 2010; revised December 8, 2010; accepted December 19, 2010. Date of publication February 6, 2011; date of current version May 20, 2011. This work was supported by the European Space Agency Research Fellowship.

C. Domenech was with the Mission Science Division, Atmospheric Section, European Space Research and Technology Centre, European Space Agency, 2200 AG Noordwijk, The Netherlands. He is now with the Institute for Space Sciences, Free University of Berlin, 12165 Berlin, Germany (e-mail: carlos.domenech@wew.fu-berlin.de).

T. Wehr is with the Mission Science Division, Atmospheric Section, European Space Research and Technology Centre, European Space Agency, 2200 AG Noordwijk, The Netherlands (e-mail: Tobias.Wehr@esa.int).

Color versions of one or more of the figures in this paper are available online at http://ieeexplore.ieee.org.

Digital Object Identifier 10.1109/TGRS.2010.2102768

methodologies based on simulated databases are limited and difficult to extrapolate to real situations. Following the same line, the BBR thermal-flux-retrieval algorithm was developed using theoretical ADMs [6]. The reduced anisotropic effect in the longwave (LW) domain makes the use of theoretical models easier. In that study, a synthetic database of spectral radiances is computed using RT calculations. Then, the combination of both nadir and off-nadir observations into a modelled effective radiance, and the correlation between the angular and the spectral behaviour of the radiation field are exploited to develop the retrieval algorithms.

In principle, the creation of a sufficiently large satellite BBR-like database that accomplishes the BBR viewing requirements would allow building an empirical ADM. However, given the peculiarity of the BBR AT geometry, it is not possible to obtain enough angular sampling to perform the hemispheric radiance integration. Thus, the selection of a representative satellite data set does not permit the construction of BBR angular models. An alternative solution would be to use existing angular models. The Clouds and the Earth's Radiant Energy System (CERES) instrument [7] employs ADMs constructed from data observed by CERES itself. The CERES rotating azimuth capability used to sample the anisotropic radiance field from all directions provides a greatly adequate data set from which to develop ADMs [8], [9]. By using the sorting-into-angular-bins approach, a large ensemble of observations is sorted into discrete angular ranges and parameters that define an angular bin. Then, the radiative flux is computed for every bin. Each of those bins is defined by the surface type and atmospheric parameters that are distinguishable by the onboard multispectral imager. Considerable efforts have been devoted to improve these angular models [10], [11]. However, ADMs are sensor dependent, i.e., they are influenced by the spatial resolution of the sensor and the satellite orbit, which is also a sampling issue. For instance, the CERES Protoflight Model onboard the Tropical Rainfall Measuring Mission (TRMM) acquired radiances from a 35° inclined orbit, thus providing sampling in the tropical region only. This constrains the creation of an angular model applicable to the whole planet. The sampling is biased and unacceptable for the polar low Earth orbit defined for EarthCARE. The CERES Terra angular models [9] would be a better solution for the SW BBR flux derivation. Nevertheless, the Terra ADM cannot be easily adapted to the BBR due to the great complexity of the algorithm. Thus, the artificial neural network (ANN) method described by Loukachine and Loeb [12], [13] and used in ScaRaB-3 by Viollier *et al.* [14] has been adopted and further develop for the L2 BBR SW flux-retrieval algorithms. The ANN performance has been optimized by testing three different architectures with three hidden neuron layers, namely, feed-forward, cascade forward, and a customized-forward network and trained all of them with backpropagation. The network is constructed as function of the solar zenith angle (SZA), the three quasi-instantaneous BBR measurements, and the coincident imager measurements over the BBR field of view (FOV).

Three different ADM schemes have been considered in this paper, defining the angular bins by their surface type, sky conditions, and CERES scene identification parameter (CERES ID). Thus, the BBR-like database of CERES data has been sorted by those conditions and then stratified in the four input variables (SZA, forward, backward, and nadir SW radiances) to build up three different training data sets.

This study is limited to the SW domain, the most critical case. An exhaustive error analysis has been done by comparing ANN-derived TOA fluxes with TOA fluxes obtained from CERES Terra ADMs and the most optimized network, and the adequate ADM classification scheme has been selected. The BBR ANN-based ADM shows results compliant with the EarthCARE requirements for many different conditions when applied to the 2×10^6 CERES observations collected during the study.

III. CERES BBR-Like Data

The CERES data employed in the construction of the ANN training data sets have to simulate the forthcoming EarthCARE BBR observations, i.e., the angular viewing geometry and the spectral-band specification designed for the instrument. In particular, there is a CERES data product that fulfills the requirements: CERES Single Scanning Footprint TOA/Surface Fluxes and Clouds (SSF) Edition2B-Rev1. Each SSF file contains footprints from a single hour (which is approximately two-thirds of an orbit) of CERES BB unfiltered radiances, scene type, derived fluxes, and viewing geometry. However, not all these CERES acquisitions are useful for this study. Three BB quasi-instantaneous radiances pointing to the same scene at nadir and $\pm 50^\circ$ are a request; thereby, only radiances acquired in AT scanning after the Earth-rotation correction patch [15] is applied can be valid. Otherwise, the AT colocation between the off-nadir views is hardly possible to achieve.

Eight days of CERES AT data have been employed in this paper, namely, two days for January 2005: January 11 and 25 (not corrected AT scanning) and six days for February 2005: February 8, 22, 25, 26, 27, and 28 (true AT (TAT) scanning). The TAT scans in February 2005 were incited by the ESA study [16] with a specific instrument coverage request. The CERES instrument (FM2) used to switch to AT operation mode during daytime every 15 days. However, different problems regarding the early aging of the CERES sensor led to the decision to restrict the CERES scanning modes to cross-track mode. Thus, the entire data set of CERES TAT data available at the National Aeronautics and Space Administration (NASA) Atmospheric Sciences Data Center (ASCD) is analyzed in this study.

The TAT CERES data sets are scanned to select the CERES BBR-like data. It is necessary to find spatial/temporal collocated observations in the nadir and off-nadir backward and forward views. The algorithm selects oblique and nadir angles between 45° and 55°, and 0° and 5°, respectively, being the relative azimuth between the off-nadir views in the range [170–190] degrees. The distance between FOV centers of those measurements is forced to be less than 10 km. Several filters have been applied to verify the consistency between nadir and off-nadir radiances, specifically, over the cloud-classification parameter (parameter to identify the cloud type) and the CERES ID for the nadir and off-nadir targets. The coherence in the CERES-derived fluxes is evaluated as well. The bias between the CERES off-nadir flux estimates (theoretically equal) is computed, and the system filters the data when the bias exceeds

5% of the maximum flux estimated for the target. At the end, a large data set of SW CERES triplets that reproduces the BBR acquisitions (hereafter called as BBR-like CERES database) has been collected and thoroughly filtered to avoid noise.

IV. Flux Estimation

A neural network has been trained with specific training sets in order to obtain ANN-based SW fluxes from CERES BBR-like measurements. Moderate-Resolution-Imaging-Spectroradiometer-based cloud and aerosol properties convolved over the CERES FOV [17] are used to create and test several schemes of scene definitions. After an adequate training, the ANN is capable of reproducing the original CERES flux estimates (inferred from CERES Terra ADMs [9]). Then, the ANN-based ADM is ready to operate as a scene-dependent function of four input variables. The ADM scene type is selected based on the particular ADM scheme employed, while the SZA and the three BB SW radiances are used as inputs for the conversion procedure

$$F_{\mathrm{ANN}} = f(\theta_0, L_0, L_{+50}, L_{-50}, \mathrm{scene}) \tag{1}$$

where F_{ANN} is the ANN-derived TOA flux, scene refers to the combination of surface type (which does not depend on imager retrieval) and atmospheric properties (which depends on imager retrievals), θ_0 is the SZA, and L_0, L_{+50}, and L_{-50} are the measured BB radiances for nadir, forward, and backward views, respectively. The viewing zenith angle and relative azimuth angle are fixed due to the BBR viewing geometry.

V. Backpropagation Neural-Network Structure

This section describes the backpropagation network architectures used to characterize the CERES Terra ADMs. Backpropagation is the generalization of the Widrow–Hoff learning rule to multiple-layer networks. Input vectors and the corresponding target networks are used to train a network until it can approximate a function that associates the input vectors with specific output vectors. The standard backpropagation is a gradient descent algorithm in which the network weights are moved along the negative of the gradient of the performance function.

This technique has been widely used in the atmospheric community, Chevallier *et al.* [18] employed the *NeuroFlux* scheme to derive the LW radiative budget, Yongxiang *et al.* [19] described the narrow-to-broad radiance conversion using a neural network, Loukachine and Loeb [12] reproduced the CERES TRMM ADMs with a feedforward error backpropagation network, and Loukachine and Loeb [13] applied the same methodology to the CERES Terra ADMs to deal with CERES FOV with insufficient imager information. Recently, Viollier *et al.* [14] have adopted the ANN method described by the CERES team, replacing the BB radiances by narrowband radiances from the auxiliary channels of ScaRaB as input variables of the model.

A general layout of one-hidden-layer network is shown in Fig. 1. Neural networks usually have one or more hidden layers

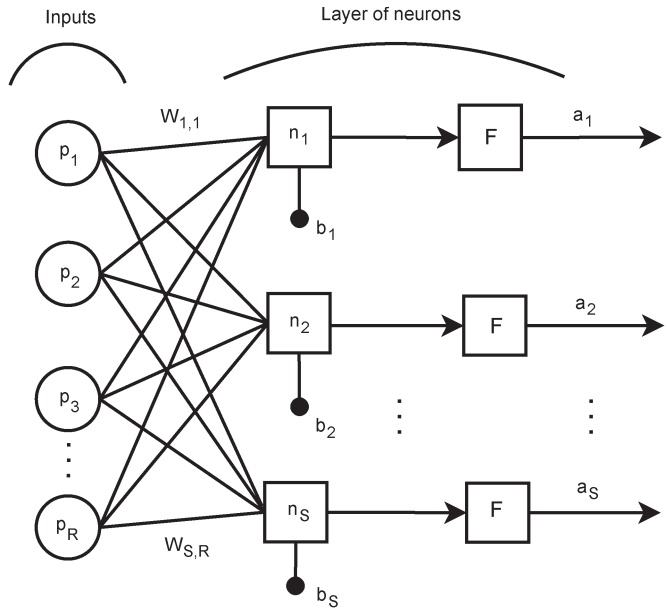

Fig. 1. One-layer network structure with R input elements (p) and S neurons (n): weight (W), bias (b), transfer function (F), and output (a).

of sigmoid neurons followed by an output layer of linear neurons. Each neuron of the nth layer is connected with all neurons of the previous layer with an assigned weight. The sum of the weighted inputs and the bias forms is the input to the transfer function. Multiple layers of neurons with nonlinear transfer functions allow the network to learn nonlinear relationships between input and output vectors.

Three different network architectures have been performed for this study. In particular, the angular models have been optimized for a feedforward network structure, a cascade-forward network structure and a custom-forward network structure. To reduce the number of neurons (and computational time), at least two hidden layers have been used in every ANN [25]. The neurons in the hidden layers use a tan-sigmoid transfer function and a linear transfer function in the last layer.

The four ANN input variables are the SZA and the three BBR-like CERES radiances. These are introduced in two input vectors to distinguish the different anisotropy dependence of the radiance field to the variables. Specifically, the nadir, forward, and backward radiances are grouped in a vector input, and the SZA is included in a second vector input.

A. Feedforward ANN

The feedforward network is commonly employed to approximate nonlinear problems. It can approximate a complex function (with a finite number of discontinuities) with arbitrary accuracy, given enough number of neurons in the hidden layers. The network of this study has been constructed for two input vectors with two hidden neuron layers and one output neuron layer.

Fig. 2 shows the feedforward scheme employed to create the network. The rectangles show the layer neurons, and the input/outputs are indicated by circles. The two vector inputs are connected to the first hidden layer of five neurons, Layer 1.

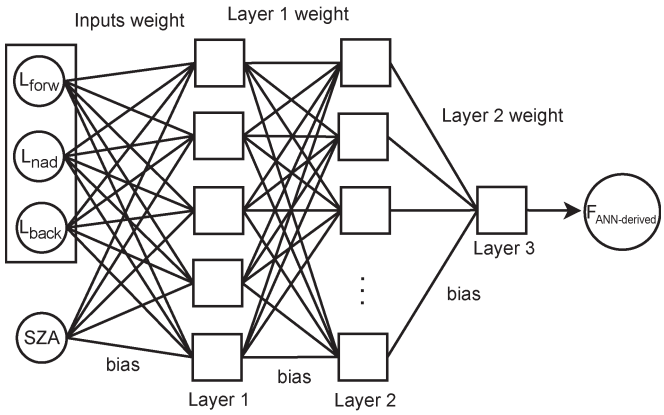

Fig. 2. Feedforward network structure with error backpropagation. Circles show the four normalized inputs introduced by two vector inputs, and rectangles show the ANN neurons, which form two hidden layers, Layer 1 and Layer 2, of 5 and 11 neurons, respectively, and the output layer, Layer 3.

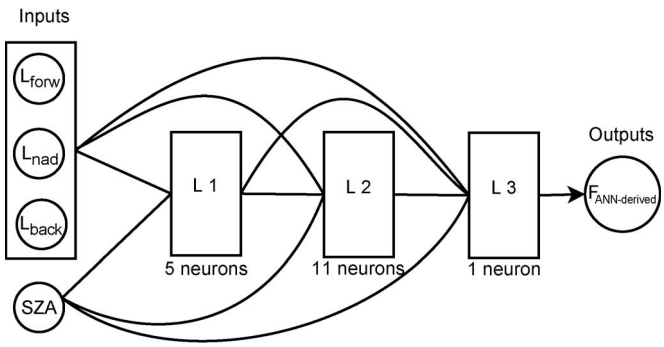

Fig. 3. Simplified scheme of the cascade-forward network structure. Rectangles represent the layer neurons, and circles represent the inputs/outputs of the system. L1 and L2 correspond to hidden layers with hyperbolic tangent sigmoid transfer functions, and L3 is an output layer with a linear transfer function.

The output of Layer 1 is connected to the second layer of 11 neurons. An output layer with a linear transfer function receives the Layer 2 weights and provides the flux estimates. A random bias is defined in every layer.

B. Cascade-Forward ANN

A cascade-forward network with three layers (two hidden layer + one output layer) has been built as well. Cascade-forward ANNs are similar to feedforward networks but include a weight connection from the input to each layer and from each layer to the successive layers. The network used in this study has connections from Layer 1 to Layer 2, Layer 2 to Layer 3, and Layer 1 to Layer 3. There are also connections from the inputs to all three layers.

Fig. 3 represents the cascade-forward ANN architecture analyzed in this section. The layout has been abbreviated to clearly show the connections. The hidden layers, Layer 1 and Layer 2, have been defined with 5 and 11 neurons, respectively.

C. Custom-Forward ANN

The custom-forward network is a feedforward ANN where the input and layer connections has been altered for our purposes. The ANN inputs are partially connected to the first and second layers. The reason for this division is to separate the anisotropic contributions of the input parameters. The four inputs, radiances and geometry, are connected to the first layer of five neurons, whereas the two neurons of Layer 2 are only connected to the SZA. The SW flux is strongly dependent on the four parameters, but it has been proved that the network performs better if this strong correlation is separated into these two branches.

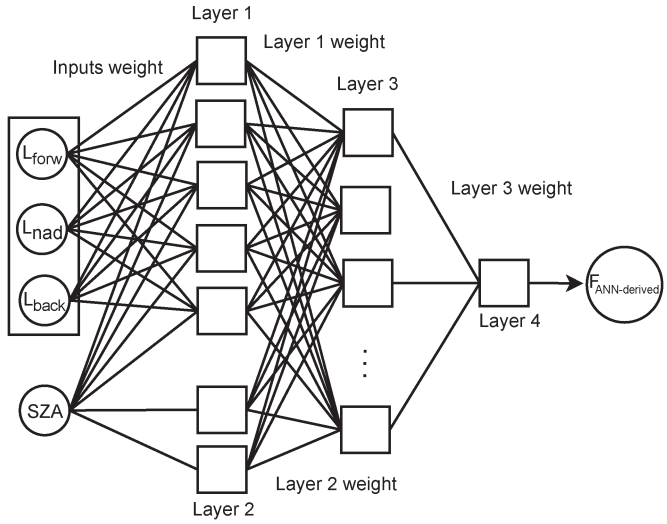

Fig. 4. Feedforward customized network structure. Four layers are used in the ANN, namely, three hidden layers, Layer 1, Layer 2, and Layer 3, with 5, 2, and 11 neurons, respectively, and the output layer, Layer 4.

TABLE I
INPUT VARIABLES, STRATIFICATION INTERVALS, AND NORMALIZATION FACTOR FOR THE TRAINING SETS

Variable	Number of bins	Bin width	Normalization
SZA	9	10°	90°
L_{forw}	30	10 $W{\cdot}m^{-2}{\cdot}sr^{-1}$	350 $W{\cdot}m^{-2}{\cdot}sr^{-1}$
L_{nad}	30	10 $W{\cdot}m^{-2}{\cdot}sr^{-1}$	350 $W{\cdot}m^{-2}{\cdot}sr^{-1}$
L_{back}	30	10 $W{\cdot}m^{-2}{\cdot}sr^{-1}$	350 $W{\cdot}m^{-2}{\cdot}sr^{-1}$

The custom-forward layout is shown in Fig. 4. The first and second hidden layers are connected to the third layer, and the third is connected to the output layer. The ANN is connected to the external world by the output layer.

VI. TRAINING

Having all network weights and biases initialized, the ANN is prepared for training. There are many variations of the backpropagation algorithm, and it is difficult to know *a priori* what will be best suited for a specific problem. It depends on many factors, the complexity of the problem, the number of data points, the error goal, etc. After testing several high-performance algorithms, the Levenberg–Marquardt training algorithm [20] seemed to be the best option. The algorithm shows the fastest convergence, and it is recommended when very accurate training is required. To prevent overfitting, the early stopping technique with random data division is employed in the training. The input data set is randomly divided so that the network is trained on the 60% of the training data until its performance begins to decrease on the validation data (20% of

TABLE II
ENTRY VECTORS IN THE TRAINING SETS AND NUMBER OF CERES FOOTPRINTS EVALUATED IN EVERY SCENE TYPE FOR THE THREE ADM SCHEMES EMPLOYED

ADM scheme 1	*ocean*	*land*	*snow/ice*
Entry vectors	2 738	1 588	641
CERES FOVs	1 361 155	413 742	155 224

ADM scheme 2	*clear*	*cloudy*
Entry vectors	873	2 899
CERES FOVs	522 449	1 407 672

ADM scheme 3	*clwat*	*clmostwat*	*clland*	*clmostland*	*cldwat*	*cldmostwat*	*cldland*	*cldmostland*	*clcldsnow*
Entry vectors	38	18	227	45	2 718	389	1 489	313	638
CERES FOVs	141 968	2 433	221 516	1 308	1 204 072	12 682	182 344	8 574	155 224

the samples). The last 20% is assigned to the test set which gives a completely independent test of network performance.

A. Training Sets

A useful BBR-like CERES data set which contains almost two million CERES footprints can be obtained from the CERES satellite data. The high computational cost of the ANN training makes it impossible to use directly the whole volume. It is then necessary to create compact training sets. However, the ANN-based ADM needs to faithfully represent all kind of atmospheric scenes. Thus, it is important to construct training sets large enough to represent the complexity of the data and obtain a high degree of generalization [12]. This can be achieved if the data set is stratified in the variable of interest, and the corresponding mean is computed.

For the atmospheric/surface scene, SW radiance and sun position are the parameters with the highest influence in the flux anisotropy considering that the relative azimuth and viewing zenith angles are fixed due to the BBR viewing geometry. Those are the parameters selected in the CERES ANN-based ADMs [12], [13], but the BBR is allowed to go one step further in the ADM building. Due to the multipointing capability, three measurements are obtained for the same target. This can be used for a better scene anisotropy representation and to infer more accurate fluxes. Thus, the ANN input variables selected are the following: SZA, CERES nadir, and forward and backward unfiltered radiances. To create the training sets for these constituents, the CERES database is stratified by these variables using the intervals shown in Table I. The number of intervals and their widths are chosen by a compromise between reducing natural noise, keeping good representation of the data, and the required computer processing time for the training process. Once the ADM scene scheme is defined, for every scene type and in every interval, the mean and standard deviation (STD) of the original CERES apparent fluxes and the mean of all four variables are calculated. A minimum of five CERES footprints is required in every data bin. The means of the input variables are normalized to their maximum allowed value in the training set, as shown in Table I, in order to avoid operations with large numbers in the process of network training.

Actual fluxes are ideal output target in the ANN training; however, they are not known. Instead, the CERES Terra flux estimates are employed. Three fluxes are collected for every footprint corresponding to the three BBR views. To reduce noise, the training data set is filtered according to the flux dispersion in the bins. An upper limit of 8% is set for the relative STD of the three angle-biased fluxes within the same bin. The exclusion of noisy data from the training sets helps to use more appropriate data to train the networks. Considering that fluxes estimated from off-nadir views ($\pm 50^\circ$) are more accurate in cloudy-sky conditions than those obtained from nadir [21], [22], mean flux values are computed only with the oblique views. The flux values are also normalized to the maximum CERES flux expected (950 $\mathrm{W \cdot m^{-2}}$) in order to optimize the network performance.

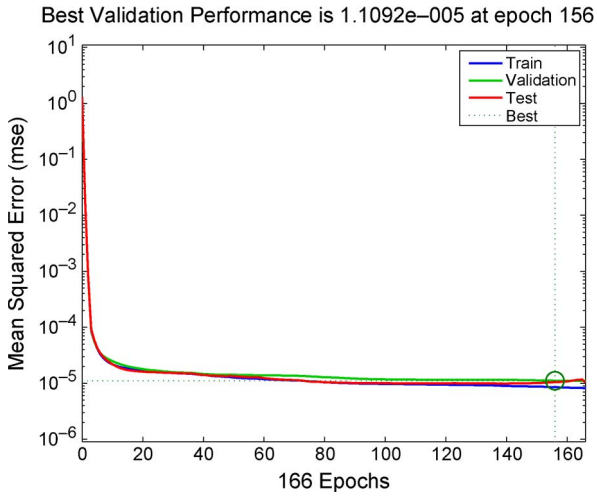

Fig. 5. Inputs and targets are divided into three sets. Of the vectors, 60% are used to train the network, 20% are used to validate how well the network performs, and the last 20% provide an independent evaluation of network performance with data that the network does not know.

B. ADM Scene Schemes

The angular models are obtained for specific scene types in order to optimize the performance of the flux conversion. The scene ID required to use the models and the ability of the models to characterize the target anisotropy are the factors to be considered in the scene selection. Three scene schemes have been created employing the CERES ADM ID. This CERES classification is composed of 11 classes:

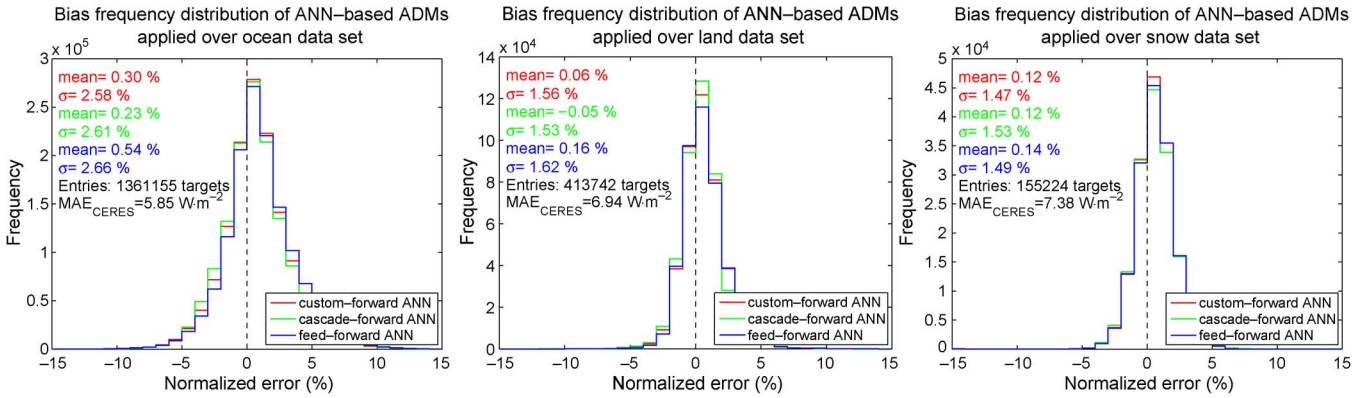

Fig. 6. Error-frequency-distribution histograms for the ADM scheme 1.

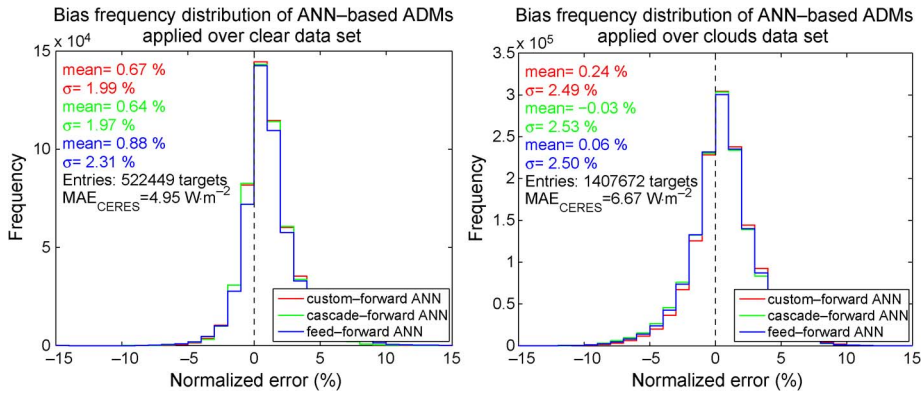

Fig. 7. Error-frequency-distribution histograms for the ADM scheme 2.

Clear water (*clwat*), Clear Mostly Water + Land/Desert/Snow (*clmostwat*), Clear Land/Desert (*clland*), Clear Mostly Land/Desert + Water/Snow (*clmostland*), Clear Mostly Snow + Water/Land/Desert (*clmostsnow*), Clouds Over Water (*cldwat*), Cloudy Mostly Water + Land/Desert/Snow (*cldmostwat*), Clouds over Land/Desert (*cldland*), Cloudy Mostly Land/Desert + Water/Snow (*cldmostland*), Clear Snow and Cloudy (*clcldsnow*), and Cloudy Mostly Snow + Water/Land/Desert (*cldmostsnow*). In particular, the training sets have been stratified as follows:

1) ADM scheme 1. Three wide training sets have been constructed in this scheme corresponding to the CERES surface types. The scheme is composed of ocean, land, and snow/ice surfaces. Cloudy conditions are not considered and belong to the statistical background data. The scene identification would not require information from the imager.
2) ADM scheme 2. In the second scheme, the scene types are defined as a function of the atmospheric conditions, namely, clear sky or cloudy sky. It is assumed that the effect of bidirectional surface reflectance is less important than cloud anisotropy in the anisotropic nature of scenes. This scheme depends on the imager retrievals to identify the scene.
3) ADM scheme 3. The third scheme is a set of nine types that corresponds to the 11 CERES ID definitions. Clouds, as well as surface properties, are taken into account in this scene definition. The *cldmosland* and *cldmostsnow* scene types are not considered in the study because not enough data were found to reach the sampling threshold. In this case, imager-retrieved products would be necessary to select the angular model.

The number of entry vectors in the training sets and the number of CERES footprints for every scene type are shown in Table II.

C. ANN Training

Once the ADM schemes are defined and the training sets constructed, the networks are ready to be trained. The three ANNs are trained using the Levenberg–Marquardt algorithm in every training subset. The weights and biases have to be initialized before training the network, and each time the ANN is initialized, the network parameters are different and might produce different solutions. Therefore, 50 networks corresponding to 50 different initializations have been trained for every considered architecture.

After training the networks for every training data set, 800 trained neural networks are obtained corresponding to the 3, 2, and 11 training sets of the ADM schemes 1, 2, and 3, respectively. Fig. 5 shows an example of an output plot after training the network. The plot shows the mean-square error of the network starting at a large value and decreasing to a smaller value, i.e., it shows that the network is learning. An exhaustive error analysis is necessary to carry out to determine the network and the ADM scheme that provide the best performance.

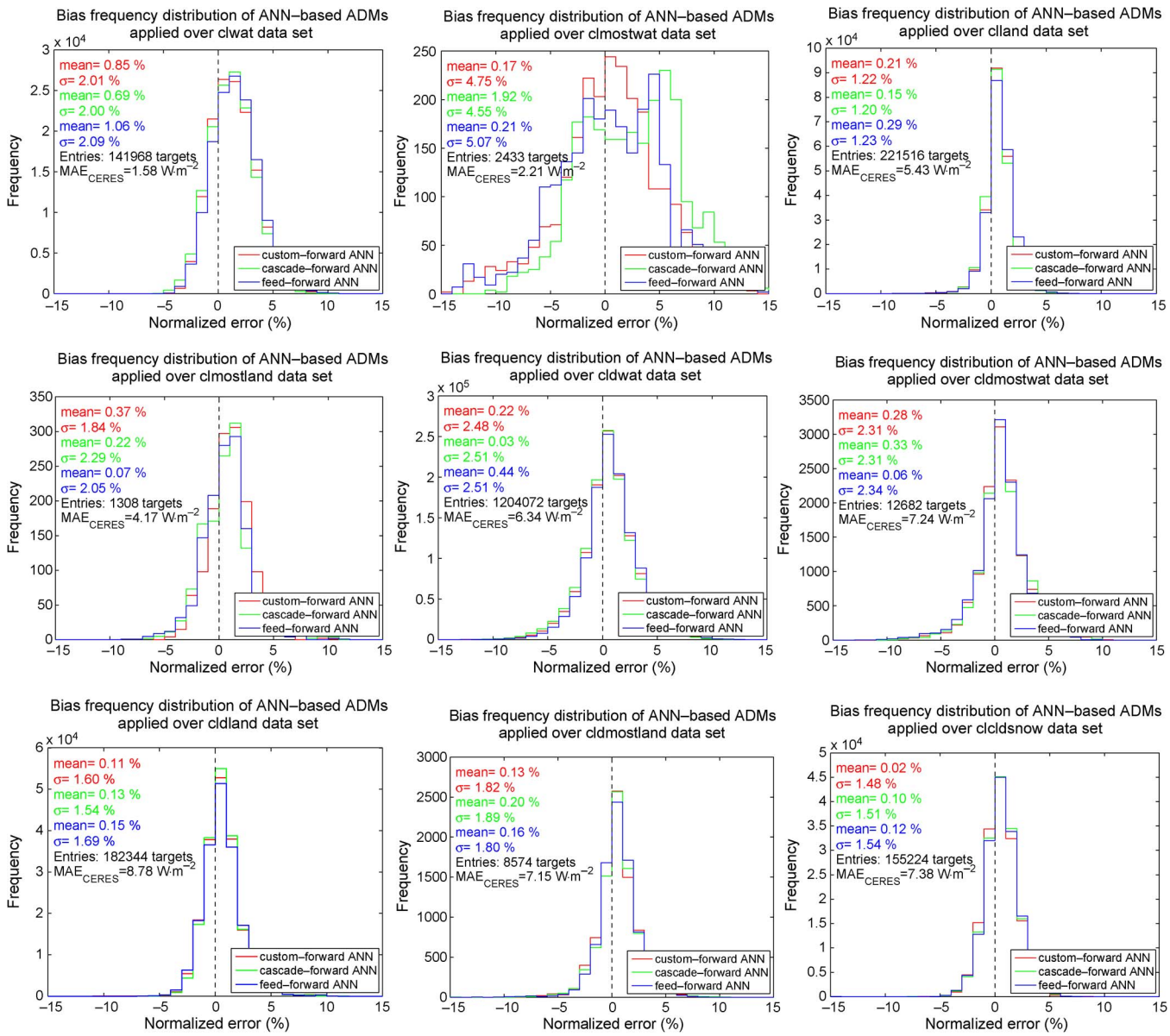

Fig. 8. Error-frequency-distribution histograms for the ADM scheme 3.

VII. Results and Validation

The validation of results and selection of the best ANN architecture and ADM scene scheme have been done by employing CERES original radiance measurements and the corresponding retrieved fluxes. In order to select the most optimized model from the 50 networks constructed for each backpropagation architecture, the root-mean-square (rms) error between the ANN-derived and mean CERES fluxes is calculated for every network over the entire BBR-like database. First, it is necessary to estimate the ANN-derived fluxes. This is done by creating the input vectors, normalizing the input and output variables to the factors used to create the training sets (Table I). Then, the normalized input data are propagated through the trained ANN, and finally, the normalization of the output is reversed to obtain the estimated flux. Only one ANN is selected for each architecture and per training set after this initial error analysis.

A. ANN Architecture Selection

The next step is to evaluate the three architectures over the entire CERES BBR-like database and select the most appropriate layout for every scene type. Figs. 6–8 show the frequency-distribution histograms of the normalized bias between ANN-based and mean CERES fluxes for every scene class used in the three ADM schemes. The mean and the STD of the distribution and the mean absolute error (MAE) between CERES flux estimates obtained for the forward and backward off-nadir views are plotted in the figures to interpret the results.

The plots show satisfactory results for all three ANN architectures, and none can be ruled out without further studies. Results for the three architectures show that ANN-derived fluxes tend to slightly overestimate the original CERES estimates. The networks perform particularly well over broad data sets. However, as expected, higher errors are obtained when they

TABLE III
ANN MODEL PERFORMANCE FOR ADM SCHEME 1

ANN	STD_{min} ($\mathrm{W{\cdot}m^{-2}}$)	RMS ($\mathrm{W{\cdot}m^{-2}}$)	BIAS ($\mathrm{W{\cdot}m^{-2}}$)	MFB (%)	MAE ($\mathrm{W{\cdot}m^{-2}}$)	MFE (%)	MAE_{CERES} ($\mathrm{W{\cdot}m^{-2}}$)
ocean							
custom-forward	6.712	4.981	0.382	0.262	3.728	1.902	5.848
cascade-forward	6.701	4.964	0.314	0.194	3.735	1.930	5.848
feed-forward	6.709	5.004	0.541	0.499	3.786	1.979	5.848
land							
custom-forward	6.575	4.217	–0.160	0.044	3.177	1.159	6.939
cascade-forward	6.539	4.128	–0.239	–0.064	3.075	1.126	6.939
feed-forward	6.599	4.318	0.016	0.144	3.286	1.208	6.939
snow							
custom-forward	5.633	4.584	0.330	0.106	3.438	1.114	7.379
cascade-forward	5.605	4.722	0.291	0.110	3.547	1.158	7.379
feed-forward	5.602	4.609	0.361	0.125	3.472	1.127	7.379

are applied over data sets with less amount of targets or for individual samples. Remarkably, for the case of coastline in clear-sky scenes (*clmostwat*), even though the CERES bias is small, deviations up to 5% are found. Bertrand *et al.* [23] formerly observed high flux uncertainties for coastal zones. The proposed network architectures show a different performance depending on the scene type. In particular, feedforward network works slightly worse than the other two models in the ADM scheme 1. The same argument can be applied to the ADM scheme 2. More variability is found in the ADM scheme 3, nevertheless the cascade-forward and custom-forward architectures show a bit more accurate flux estimations. It is important to note that the CERES flux MAE is usually higher than the MAE obtained between the original CERES and ANN-based flux estimations, which is a great estimator of the good performance of the developed ANN-based angular models.

A routine to calculate a number of error metrics to select the network with the best performance for each ADM scheme has been constructed. The error metrics considered are the rms, normalized rms error, STD(MAE), MAE, normalized mean bias, normalized mean error (NME), mean fractional bias, mean fractional error (MFE), the bias, and the intrinsic uncertainty of the target ADM ($\mathrm{STD}_{\min}$). The intrinsic error associated to each ANN can be inferred from

$$\mathrm{STD}_{\min} = \sqrt{\overline{\mathrm{STD}(F_{\mathrm{forw}})}^2 + \overline{\mathrm{STD}(F_{\mathrm{back}})}^2 + \mathrm{STD}(\mathrm{MAE})^2} \quad (2)$$

where the $\overline{\mathrm{STD}(F_{\mathrm{forw}})}$ and $\overline{\mathrm{STD}(F_{\mathrm{back}})}$ are the averages in every training set of the CERES fluxes STDs obtained from forward and backward views, respectively. The $\mathrm{STD}(\mathrm{MAE})$ is the STD of the difference in every training set between the ANN-derived and mean CERES fluxes after training the networks. As an example, Table III summarizes the results achieved for the ADM scheme 1. A detailed description of these error statistics can be found in Boylana and Russell [24]. The neural network presenting the highest number of minimum errors is selected and stored. At the end of the process, a single ANN is chosen for every ADM scheme and for each scene type.

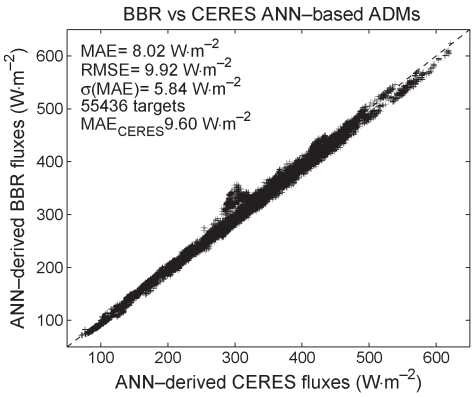

Fig. 9. Flux-estimate comparison between CERES and BBR ANN-derived ADMs.

B. CERES Neural Network ADM

In the CERES BBR-like database building process, CERES flux estimates obtained from neural-network-based ADMs [13] were not used. The current ANN-derived ADMs have been constructed without considering those models; only flux measurements inferred from the empirical CERES Terra angular models were employed. However, the CERES ANN-based flux data collected that fulfill the BBR viewing-geometry requirements can be employed to be compared with the flux retrievals computed with the ANN BBR ADMs. This comparison is meaningful because both angular models share the same methodology.

Fig. 9 shows the comparison between fluxes derived from the networks selected in the ADM scheme 1 and fluxes obtained by the direct application of the CERES ANN-based ADM. RMS errors up to 10 $\mathrm{W \cdot m^{-2}}$ are obtained; however, these results are coherent with the high discrepancies found between CERES fluxes obtained from forward and backward views (around 10 $\mathrm{W \cdot m^{-2}}$).

C. ADM Scheme Selection

The three schemes have been intercompared to decide which is the most efficient ADM scene definition for the BBR flux retrieval. The CERES BBR-like database is classified according to the CERES ID, then the ANN models, corresponding to schemes 1 and 2, are applied over the original CERES

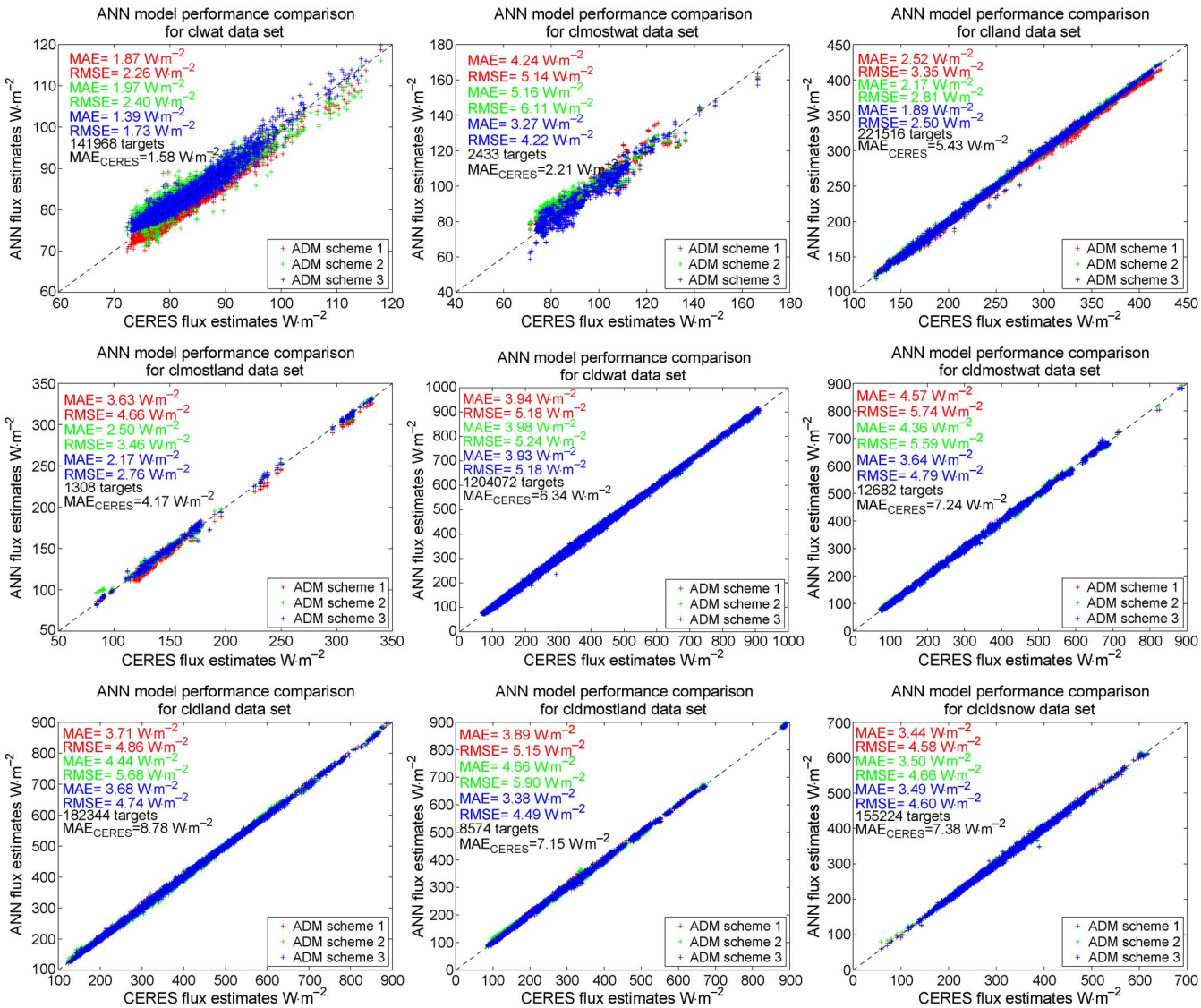

Fig. 10. Flux comparison between BBR ANN-derived estimates of scene data sets classified according to the CERES ID.

measurements, and the mean rms error and MAE are computed for every scene type. The performance of the three ANN-based angular models is shown in Fig. 10. In general, the three models show a high correlation with respect to the CERES flux estimates and present MAEs that are much lower than the MAE values computed for the CERES oblique fluxes. The three ANN models show their best results when they are applied over clear homogenous scenes (clwat and clland scene types), while the heterogenous scenes (clmost and cldmost scene types) provide the worst matches.

The error metrics used in the previous sections have been computed for every subset in order to select the most appropriate ADM scheme and quantify the error. Table IV summarizes the results obtained for every scene type. ε expresses the relative error with respect to the best accuracy obtained with the rms estimator, i.e., the improvement of the best model compared with the other two methods. As expected, networks from ADM scheme 3 guarantee the most accurate results since those models have been built from training sets corresponding to those specific scene types. However, individual high errors (outliers) are less significant when the error metrics are calculated for data sets with high number of entries; thus, the model performance show similar results in the three ADMs. This can be observed in cloudy ocean scenes. A similar behavior is found again when the models are applied over snow/ice surfaces. In this case, the difficulty to obtain useful data sets around the poles causes the high errors of the three models. A more efficient angular sampling would be needed to improve the network-training results.

According to these results, scheme 2 provides slightly lower error values than scheme 1 mainly in clear-sky land surfaces. However, the network models of ADM scheme 1 show significant better results than models from the ADM scheme 2 over clear ocean and cloudy land surfaces. Thus, considering that scheme 1 ADMs are a BBR stand-alone algorithm, i.e., only BBR radiance measurements are needed to convert radiances into radiative fluxes, and the right results obtained with scheme 1 in the comparison with the results from ADMs scheme 2, it seems clear that the ADMs from scheme 2 can be discarded. Therefore, only angular models from ADM

TABLE IV
ERROR METRICS OF THE ANN-BASED BBR ADMS OVER SCENES SORTED BY THE CERES ID PARAMETER

ADM scheme	STD_{min} ($W \cdot m^{-2}$)	RMS ($W \cdot m^{-2}$)	BIAS ($W \cdot m^{-2}$)	MFB (%)	MAE ($W \cdot m^{-2}$)	MFE (%)	ε(RMS) (%)
clwat							
ADM scheme 1	2.526	2.261	-1.522	-1.843	1.871	2.267	23.34
ADM scheme 2	2.670	2.403	1.202	1.531	1.973	2.396	27.86
ADM scheme 3	2.089	1.733	0.524	0.670	1.393	1.681	–
clmostwat							
ADM scheme 1	4.528	5.137	2.721	3.254	4.238	4.716	17.78
ADM scheme 2	4.451	6.114	4.113	4.871	5.163	5.833	30.92
ADM scheme 3	4.089	4.223	0.007	0.057	3.274	3.661	–
clland							
ADM scheme 1	5.244	3.349	-0.938	-0.306	2.517	1.079	25.39
ADM scheme 2	4.903	2.814	0.708	0.379	2.166	0.991	11.18
ADM scheme 3	4.809	2.499	0.260	0.141	1.888	0.868	–
clmostland							
ADM scheme 1	4.849	4.656	-2.800	-1.777	3.629	2.386	40.61
ADM scheme 2	4.303	3.456	0.472	0.511	2.502	1.784	20.01
ADM scheme 3	4.063	2.765	0.564	0.351	2.171	1.449	–
cldwat							
ADM scheme 1	6.728	5.182	0.522	0.418	3.945	1.880	–
ADM scheme 2	6.768	5.241	0.275	0.186	3.980	1.875	1.12
ADM scheme 3	6.714	5.185	0.132	0.003	3.929	1.849	0.05
cldmostwat							
ADM scheme 1	5.646	5.739	0.637	1.201	4.574	2.395	16.54
ADM scheme 2	5.675	5.594	0.304	0.823	4.357	2.112	14.38
ADM scheme 3	5.352	4.790	0.393	0.257	3.636	1.654	–
cldland							
ADM scheme 1	6.639	4.861	0.565	0.218	3.710	1.156	2.40
ADM scheme 2	6.821	5.684	0.467	0.284	4.445	1.467	16.54
ADM scheme 3	6.574	4.744	0.212	0.117	3.681	1.146	–
cldmostland							
ADM scheme 1	6.081	5.147	1.105	0.467	3.891	1.519	12.78
ADM scheme 2	6.160	5.899	1.677	1.197	4.660	2.150	23.89
ADM scheme 3	5.697	4.489	0.177	0.112	3.379	1.346	–
clcldsnow							
ADM scheme 1	5.640	4.584	0.330	0.106	3.438	1.114	1.56
ADM scheme 2	5.815	4.657	0.071	0.051	3.496	1.145	0.27
ADM scheme 3	5.672	4.596	0.011	0.007	3.491	1.129	–

schemes 1 and 3 are recommended for the BBR algorithm implementation. Thus, operational BBR SW radiance-to-flux conversion algorithms could rely on the **ANN-based ADMs** with **scene scheme 1** when information from the EarthCARE's imager is not available, and the **ANN-based ADMs** with **scene scheme 3** is advisable when the flux-retrieval algorithm can make us of the EarthCARE Multi-Spectral Imager (MSI) in the BBR FOV due to the reliability, consistency, and accuracy of the method.

VIII. CONCLUSION

The efficiency of the ANN-derived fluxes obtained with the SW BBR angular models to reproduce the SW TOA CERES Terra fluxes has been amply demonstrated in this paper. The BBR flux retrievals accurately match the CERES ANN-based fluxes under almost all the scene types considered. In addition, two ADM scene schemes have been shown useful for a potential implementation in the BBR L2 algorithms. As conclusion of this paper, BBR stand-alone fluxes can be derived with an acceptable accuracy without imager information, and BBR imager-dependent fluxes can be obtained with higher accuracy when MSI data are available.

However, results obtained over ice/snow regions are not fully satisfactory. More efforts are needed to optimize the flux-retrieval performance in these critical surfaces. Enlarging the CERES BBR-like database by reducing the demanding requirements or by increasing the number of CERES days analyzed in polar regions could solve the problem. In the same line, the ANN-based ADM works reasonably well with coastline scenes, nevertheless, more developments are necessary to improve the results.

It is important to remark that the SW ADMs developed for the BBR rely on CERES Terra flux retrievals. The ANN-derived fluxes simulate fluxes estimated with the empirical CERES angular models, thus the accuracy expected for these BBR ADMs will always be, at best, as high as the accuracy given for the instantaneous CERES TOA fluxes. According to Loeb *et al.* [11], [22], the CERES Terra instantaneous TOA flux uncertainty of all-sky ocean and land is 6% (17 $W \cdot m^{-2}$) and 9% (26 $W \cdot m^{-2}$) in polar regions. A prototype methodology should then be developed in next studies to be aimed at

improving TOA flux accuracies in order to fulfill the overarching EarthCARE goal.

ACKNOWLEDGMENT

The authors would like to thank E. Lopez-Baeza, M. Drinkwater, N. G. Loeb, and the anonymous reviewers for their constructive and helpful comments, and to the Atmospheric Sciences Data Center at the National Aeronautics and Space Administration, Langley Research Center, for providing them with the Clouds and the Earth's Radiant Energy System Single Scanning Footprint TOA/Surface Fluxes and Clouds data product. This work was performed at the European Space Research and Technology Centre, European Space Agency.

REFERENCES

[1] "Reports for mission selection, the six candidate earth explorer missions. EarthCARE-Earth clouds, aerosols and radiation explorer," ESTEC, Noordwijk, The Netherlands, European Space Agency SP-1279(1), 2004.

[2] J. T. Suttles, R. N. Green, P. Minnis, G. L. Smith, W. F. Staylor, B. A. Wielicki, I. J. Walker, D. F. Young, V. R. Taylor, and L. L. Stowe, "Angular radiation models for earth-atmosphere system. Volume I—Shortwave radiation," NASA Langley Res. Center, Hampton, VA, NASA RP-1184, 1988.

[3] J. T. Suttles, R. N. Green, G. L. Smith, B. A. Wielicki, I. J. Walker, V. R. Taylor, and L. L. Stowe, "Angular radiation models for earth-atmosphere system. Volume II—Longwave radiation," NASA Langley Res. Center, Hampton, VA, NASA RP-1184, 1989.

[4] C. Domenech, E. Lopez-Baeza, D. P. Donovan, and T. Wehr, "Radiative flux estimation from BBR using synthetic angular models in the EarthCARE mission framework. Part I: Methodology," *J. Appl. Meteor. Clim.*, 2011, to be published.

[5] C. Domenech, E. Lopez-Baeza, D. P. Donovan, and T. Wehr, "Radiative flux estimation from BBR using synthetic angular models in the EarthCARE mission framework. Part II: Evaluation," *J. Appl. Meteor. Clim.*, 2011, to be published.

[6] C. Domenech, T. Wehr, and J. Fischer, "Towards an EarthCARE thermal flux determination: Evaluation using CERES true along-track data," *J. Geophys. Res.*, 2011. DOI: 10.1029/2010JD015212, to be published.

[7] B. A. Wielicki, B. R. Barkstrom, E. F. Harrison, R. B. Lee, III, G. L. Smith, and J. E. Cooper, "Clouds and the Earth's Radiant Energy System (CERES): An earth observing system experiment," *Bull. Amer. Meteorol. Soc.*, vol. 77, no. 5, pp. 853–868, May 1996.

[8] N. G. Loeb, N. M. Smith, S. Kato, W. F. Miller, S. K. Gupta, P. Minnis, and B. A. Wielicki, "Angular distribution models for top-of-atmosphere radiative flux estimation from the clouds and the earth's radiant energy system instrument on the tropical rainfall measuring mission satellite. Part I: Methodology," *J. Appl. Meteor.*, vol. 42, pp. 240–265, 2003.

[9] N. G. Loeb, S. Kato, K. Loukachine, and N. Manalo-Smith, "Angular distribution models for top-of-atmosphere radiative flux estimation from the clouds and the earth's radiant energy system instrument on the terra satellite. Part I: Methodology," *J. Atmos. Ocean. Technol.*, vol. 22, no. 4, pp. 338–351, Apr. 2005.

[10] N. G. Loeb, K. Loukachine, N. Manalo-Smith, B. A. Wielicki, and D. F. Young, "Angular distribution models for top-of-atmosphere radiative flux estimation from the clouds and the earth's radiant energy system instrument on the tropical rainfall measuring mission satellite. Part II: Validation," *J. Appl. Meteor.*, vol. 42, pp. 1748–1769, 2003.

[11] N. G. Loeb, S. Kato, K. Loukachine, N. Manalo-Smith, and D. R. Doelling, "Angular distribution models for top-of-atmosphere radiative flux estimation from the clouds and the earth's radiant energy system instrument on the terra satellite. Part II: Validation," *J. Atmos. Ocean. Technol.*, vol. 24, no. 4, pp. 564–584, 2007.

[12] K. Loukachine and N. Loeb, "Application of an artificial neural network simulation for top-of-atmosphere radiative flux estimation from CERES," *J. Atmos. Ocean. Technol.*, vol. 20, no. 12, pp. 1749–1757, 2003.

[13] K. Loukachine and N. Loeb, "Top-of-atmosphere flux retrievals from CERES using artificial neural networks," *Remote Sens. Environ.*, vol. 93, no. 3, pp. 381–390, Nov. 2004.

[14] M. Viollier, C. Standfuss, O. Chomette, and A. Quesney, "Top-of-atmosphere radiance-to-flux conversion in the SW domain for the ScaRaB-3 instrument on megha-tropiques," *J. Atmos. Ocean. Technol.*, vol. 26, no. 10, pp. 2161–2171, Oct. 2009.

[15] M. Capderou and M. Viollier, "True along-track scan to improve radiation budget estimations," *J. Atmos. Ocean. Technol.*, vol. 23, no. 8, pp. 1093–1103, 2006.

[16] E. López-Baeza, H. W. Barker, F. H. Berger, M. Capderou, C. Doménech, A. Lorenz, P. Raberanto, A. Velázquez, and M. Viollier, "Improvement of angular dependence models, final report," ESA/ESTEC, Noordwijk, The Netherlands, Final Rep., Contract No. 17772/04/NL/GS, 2006.

[17] P. Minnis, D. Young, S. Sun-Mack, P. Heck, D. Doelling, and Q. Trepte, "CERES cloud property retrievals from imagers on TRMM, terra, and aqua," in *Proc. SPIE—Remote Sensing of Clouds and the Atmosphere VIII*, 2003, vol. 5235, pp. 37–48.

[18] F. Chevallier, F. Cheruy, N. A. Scott, and A. Chedin, "A neural network approach for a fast and accurate computation of a longwave radiative budget," *J. Appl. Meteor.*, vol. 37, no. 11, pp. 1385–1397, Nov. 1998.

[19] Y. Hu, H. Zhang, B. Wielicki, and P. Stackhouse, "A neural network MODIS–CERES narrowband to broadband conversion," in *Proc. IEEE IGARSS*, 2002, vol. 6, pp. 3227–3229.

[20] M. Hagan and M. Menhaj, "Training feed-forward networks with the Marquardt algorithm," *IEEE Trans. Neural Netw.*, vol. 5, no. 6, pp. 989–993, Nov. 1994.

[21] A. Bodas-Salcedo, J. Gimeno-Ferrer, and E. López-Baeza, "Flux retrieval optimization with a nonscanner along-track broadband radiometer," *J. Geophys. Res.*, vol. 108, no. D2, p. 4061, 2003.

[22] N. G. Loeb, W. Sun, W. F. Miller, K. Loukachine, and R. Davies, "Fusion of CERES, MISR, and MODIS measurements for to-of-atmosphere radiative flux validation," *J. Geophys. Res.*, vol. 111, no. D18209, 2006.

[23] C. Bertrand, N. Clerbaux, A. Ipe, S. Dewitte, and L. Gonzalez, "Angular distribution models, anisotropic correction factors, and mixed clear-scene types: A sensitivity study," *IEEE Trans. Geosci. Remote Sens.*, vol. 43, no. 1, pp. 92–102, Jan. 2005.

[24] J. W. Boylana and A. G. Russell, "PM and light extinction model performance metrics, goals, and criteria for three-dimensional air quality models," *Atmos. Environ.*, vol. 40, no. 26, pp. 4946–4959, Aug. 2006.

[25] N. K. Bose and P. Liang, *Neural Network Fundamentals With Graphs, Algorithms, and Applications*. New York: McGraw-Hill, 1996.

Carlos Domenech received the M.S. degree for advanced studies in physics of the environment and thermodynamics and the Ph.D. degree with European Doctorate Mention in physics of the Earth and thermodynamics from the University of Valencia (UVEG), Valencia, Spain, in 2005 and 2008, respectively. His Ph.D. thesis was on the subject of the use of synthetic angular models for top-of-atmosphere flux retrievals of the multiangular Earth Clouds, Aerosols, and Radiation Explorer (EarthCARE) Broadband Radiometer.

He was a Research Fellow with the Mission Science Division, European Space Research and Technology Centre, European Space Agency (ESA), Noordwijk, The Netherlands, between 2008 and 2010. During his tenure with ESA, the research activity was focused on the development of EarthCARE L2 algorithms. Since August 2010, he has been with the Institute for Space Sciences, Free University of Berlin, Berlin, Germany. He is currently involved in atmospheric radiative flux-retrieval studies and Earth-radiation budget analysis.

Tobias Wehr received the Ph.D. degree in physics from the University of Bremen, Bremen, Germany, in 1996.

He worked on atmospheric radiative-transfer modeling and the retrieval of atmospheric temperature and trace gases from airborne and spaceborne passive microwave limb sounders. In 1997, he was with the Joint Center for Earth System Technology, University of Maryland, Baltimore County, where he developed fast radiative-transfer models for the High-resolution Infrared Radiation Sounder satellite instruments for the National Aeronautics and Space Administration Data Assimilation Office. Since November 1998, he has been with the European Space Research and Technology Centre, European Space Agency, Noordwijk, The Netherlands, on the selection and scientific preparation of several Earth observation satellites. Currently, he is the Mission Scientist with Earth Clouds, Aerosols and Radiation Explorer (EarthCARE), Technical Officer of several preparatory scientific activities, and convenes, together with the Japanese Aerospace Exploration Agency, the EarthCARE Joint Mission Advisory Group.